Terahertz laser vibration–rotation–tunneling spectrum of the water pentamer–d_{10}.
Constraints on the bifurcation tunneling dynamics

Jeff D. Cruzan [1], Mark R. Viant, Mac G. Brown, Don D. Lucas [2], Kun Liu [3], Richard J. Saykally [*]

Department of Chemistry, University of California at Berkeley, Berkeley, CA 94530, USA

Abstract

The vibration–rotation–tunneling (VRT) spectrum of a low-frequency intermolecular vibration of $(D_2O)_5$ was recorded near 0.9 THz (30.2 cm^{-1}). From an analysis of the relative intensities in the compact Q-branch region, the ground-state C-rotational constant is estimated to be 975 ± 60 MHz, consistent with ab initio structural predictions. The precisely determined B-rotational constant ($B = 1750.96 \pm 0.20$ MHz) agrees well with previous results. Efforts to resolve possible bifurcation tunneling fine structure, such as that observed in VRT spectra of $(D_2O)_3$, revealed no such effects. This constrains the splittings to be less than 450 kHz, or roughly 3 times smaller than required by previous results. © 1998 Published by Elsevier Science B.V. All rights reserved.

1. Introduction

Pentagonal rings of water molecules appear to be ubiquitous in nature. Clathrate hydrates and solvation of hydrophobic groups in proteins and DNA are two interesting examples of systems wherein these structures have been identified. Moreover, computer simulations of liquid water have predicted that hydrogen-bond network rearrangements (HBNR) interconvert small arrangements on a time scale much longer than that of intermolecular vibrational modes of a typical cluster, with identifiable five- and six-membered rings dominating population distribution in the HB network at any time [1].

As the prototype for a five-membered water polygon, the isolated (gas-phase) water pentamer adopts a quasiplanar pentagonal ring structure as its minimum energy form (Fig. 1). High-resolution absorption spectra of isolated water pentamers have now been measured in two distinct spectral regions using

---

[*] Corresponding author. E-mail: saykally@cchem.berkeley.edu
[1] Present address: Department of Molecular and Cellular Biology, Harvard University, 7 Divinity Avenue, Cambridge, MA 02138, USA.
[2] Present address: Department of Earth and Planetary Sciences, Massachusetts Institute of Technology, Cambridge, MA 02139, USA.
[3] Present address: Department of Chemistry; University of Southern California, Los Angeles, CA 80000, USA.
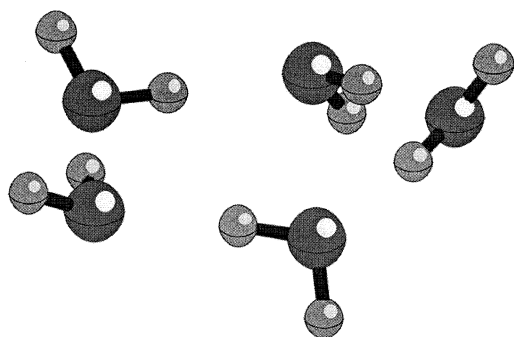
Fig. 1. The theoretically predicted minimum energy structure of the cyclic water pentamer has no point group symmetry elements. The minimum structure is puckered by $\sim 20°$, analogous to the puckered structure of cyclopentane. The equilibrium structures of several torsional variants have similar energies but the VRT experiment establishes a symmetric-top structure, which results as the asymmetric structure is vibrationally averaged to a planar (C_{5h}) structure over the facile hydrogen bond torsional motions which 'flip' the unbound protons between opposite sides of the oxygen atom framework.

Terahertz vibration–rotation–tunneling (VRT) spectroscopy. The first, a parallel symmetric rotor spectrum of $(D_2O)_5$ centered near 81.2 cm^{-1}, was reported recently [2]. The results of an analysis of a second parallel $(D_2O)_5$ spectrum centered near 30.2 cm^{-1}, the most salient feature of which is its low vibrational excitation frequency, are presented here.

Like the water trimer, the pentamer is a cyclic, chiral (C_1 symmetry), homodromic ring, with each monomer acting as a single H-bond donor and acceptor. The low-barrier H-bond torsional motion illustrated in the figure, analogous to that which occurs in the trimer [3–6] and (by inference) the tetramer [7,8], is implicated as the dominant structural rearrangement in the pentamer because the VRT experiments have measured exact symmetric rotor spectra. This reflects a vibrationally averaged structure having five equivalent monomers, unlike those of Fig. 1. Interestingly, detailed structural calculations [9] have predicted that the oxygen framework of the pentamer is puckered by as much as 20°, implying that relatively facile heavy atom (oxygen) motion must accompany the H-bond torsion to rationalize the measured symmetric structure.

Ab initio studies of the structures of small water clusters have consistently predicted such quasiplanar

cyclic structures as the global minima for $(H_2O)_n$, $n = 3,4,5$, with the hexamer structure being less certain [10]. In general, it has been shown that for clusters through the pentamer, models incorporating at least high-order multipolar electrostatic interactions are adequate to fix the general features of the global minimum structures with little ambiguity, although the structural details do not match more recent ab initio calculations. Chalasinski and coworkers [11] showed that the success of the simpler models is partly due to fortuitous cancellation of exchange and polarization interactions. It is now clear that a full accounting of the most subtle pairwise and non-additive intermolecular forces is necessary to fix the structures of water clusters larger than the pentamer, and to calculate their detailed properties.

In so far as the data allow for rigorous determinations of vibrationally averaged structures, the VRT spectra have both confirmed the ab initio structure predictions and have shown that the average interoxygen separation (R_{OO}) decreases exponentially with the number of monomers in cyclic water clusters The results indicate that R_{OO} converges to the ordered ice value by $n = 4$ or 5 for cyclic clusters [2,7,12]. The trimer and tetramer measurements have supplied additional dynamical information in the form of fine structure present in each rotation–vibration line due to quantum tunneling among degenerate structural frameworks. No such effects are present in either of the $(D_2O)_5$ VRT spectra measured thus far. These results may indicate that the increase in permonomer binding energy due to H-bond cooperativity arising primarily from the possibility of more favorable H-bonding geometries (linear H-bonds) is great enough to quench some of the possible rearrangement dynamics at the rotational temperatures accessed by the VRT experiments (~ 5 K).

In this Letter, an analysis of the FIR spectrum of $(D_2O)_5$ recently recorded near 30.2 cm^{-1} is presented. The reliability of the relative intensity information in the compact Q-branch region has allowed an improved estimate of the ground-state C-rotational constant, which helps to calibrate the experimentally observed structure with the theoretical predictions. Additionally, we present the results of an experiment to determine whether any underlying tunneling splittings could be resolved in the transitions.

2. Experimental and results

The Berkeley Terahertz spectrometers have been described elsewhere [13]. Only the details relevant to this experiment will be reported here. D_2O clusters were formed in a supersonic nozzle beam expansion of approximately 1% D_2O (99.5% purity, Cambridge Isotopes) seeded in Ar, Ne or He using the 10-cm-long pulsed planar (slit-shaped orifice) nozzle designed and recently described by Liu et al. [14]. The expansion was probed by multipassing the tunable THz radiation in front of the nozzle orifice 18 times using a Herriott cell [15] for an effective absorption path length of over 2 m. The THz laser was frequency modulated at 50 kHz and demodulated at 100 kHz by a fast lock-in amplifier (RC = 100 μs) after interaction with the expansion. The output of the lock-in amplifier was fed into a digital storage oscilloscope (Tektronix TDS320), where the absorption profile (the oscilloscope trace) was integrated by a 486-PC computer after 32 or 64 nozzle pulses (typically) were averaged.

A total of 121 transitions of a parallel ($\Delta K = 0$) vibration–rotation spectrum of an oblate symmetric rotor were recorded in the region centered around 30.2 cm^{-1} (905 GHz). They are listed in Table 1. The compact Q-branch region, clustered in groups of transitions belonging to manifolds of $K'' \rightarrow K' = K''$ transitions (Fig. 2), was markedly similar to that of the 81.2 cm^{-1} $(D_2O)_5$ VRT spectrum [2]. Preliminary isotopic substitution experiments (see Ref. [7]) indicated that the carrier contained more than four D_2O molecules. Additionally, the transitions were observed in both Ar and Ne carrier gases, ruling out these species as constituents of the chromophore. Therefore the initial assignment proceeded from the assumption that the absorber was indeed $(D_2O)_5$. Because the assignment produced numerous combination differences common with those of the 81.2 cm^{-1} spectrum, no additional isotopic substitution experiments were performed to further clarify the identify of the absorber. The simple symmetric rotor energy level expression,

$$E_{J,K}^{v} = \nu + BJ(J+1)$$
$$+ (C - B)K^2 - D_J J^2(J+1)^2$$
$$- D_{JK} J(J+1) K^2, \tag{1}$$

Table 1
Observed transitions (MHz) of the 30.2 cm^{-1} $(D_2O)_5$ spectrum

$J'_\kappa \leftarrow J''_\kappa$	Frequency (MHz)	Residual
$4_0 \leftarrow 5_0$	887 864	0.3
$4_1 \leftarrow 5_1$	887 869	0.5
$4_2 \leftarrow 5_2$	887 885	0.4
$4_3 \leftarrow 5_3$	887 911	0.3
$4_4 \leftarrow 5_4$	887 949	0.4
$3_0 \leftarrow 4_0$	891 365	1.4
$3_1 \leftarrow 4_1$	891 369	0.1
$3_2 \leftarrow 4_2$	891 385	0.1
$3_3 \leftarrow 4_3$	891 411	0.1
$2_0 \leftarrow 3_0$	894 864	-0.3
$2_1 \leftarrow 3_1$	894 869	0.0
$2_2 \leftarrow 3_2$	894 885	0.2
$2_1 \leftarrow 2_1$	905 374	-1.0
$3_1 \leftarrow 3_1$	905 375	-0.2
$2_2 \leftarrow 2_2$	905 390	-0.6
$3_2 \leftarrow 3_2$	905 392	-0.1
$4_2 \leftarrow 4_2$	905 393	-0.1
$5_2 \leftarrow 5_2$	905 395	0.1
$6_2 \leftarrow 6_2$	905 396	0.1
$7_2 \leftarrow 7_2$	905 399	0.1
$3_3 \leftarrow 3_3$	905 418	-0.9
$4_3 \leftarrow 4_3$	905 419	-0.6
$5_3 \leftarrow 5_3$	905 421	-0.3
$6_3 \leftarrow 6_3$	905 423	-0.4
$7_3 \leftarrow 7_3$	905 425	0.0
$8_3 \leftarrow 8_3$	905 428	0.1
$4_4 \leftarrow 4_4$	905 457	-0.8
$5_4 \leftarrow 5_4$	905 458	-0.6
$6_4 \leftarrow 6_4$	905 460	-0.3
$7_4 \leftarrow 7_4$	905 463	0.0
$5_5 \leftarrow 5_5$	905 507	-0.6
$6_5 \leftarrow 6_5$	905 509	-0.3
$7_5 \leftarrow 7_5$	905 511	0.2
$8_5 \leftarrow 8_5$	905 514	0.1
$9_5 \leftarrow 9_5$	905 517	0.4
$10_5 \leftarrow 10_5$	905 520	0.4
$6_6 \leftarrow 6_6$	905 568	-0.5
$7_6 \leftarrow 7_6$	905 570	-0.1
$8_6 \leftarrow 8_6$	905 573	0.4
$9_6 \leftarrow 9_6$	905 576	0.2
$10_6 \leftarrow 10_6$	905 579	0.1
$11_6 \leftarrow 11_6$	905 582	0.2
$12_6 \leftarrow 12_6$	905 585	-0.4
$13_6 \leftarrow 13_6$	905 588	-1.4
$7_7 \leftarrow 7_7$	905 640	-0.5
$8_7 \leftarrow 8_7$	905 642	-0.2
$9_7 \leftarrow 9_7$	905 645	0.1
$10_7 \leftarrow 10_7$	905 649	0.8
$11_7 \leftarrow 11_7$	905 652	0.3
$12_7 \leftarrow 12_7$	905 655	-0.2
$13_7 \leftarrow 13_7$	905 658	-0.8
$8_8 \leftarrow 8_8$	905 723	-0.4

Table 1 (continued)

$J'_\kappa \leftarrow J''_\kappa$	Frequency (MHz)	Residual
$9_8 \leftarrow 9_8$	905 726	0.0
$10_8 \leftarrow 10_8$	905 729	0.1
$11_8 \leftarrow 11_8$	905 732	0.2
$12_8 \leftarrow 12_8$	905 735	−0.4
$9_9 \leftarrow 9_9$	905 817	−0.4
$10_9 \leftarrow 10_9$	905 820	0.0
$11_9 \leftarrow 11_9$	905 824	0.3
$12_9 \leftarrow 12_9$	905 828	0.5
$13_9 \leftarrow 13_9$	905 831	0.3
$10_{10} \leftarrow 10_{10}$	905 922	−0.3
$11_{10} \leftarrow 11_{10}$	905 926	0.1
$12_{10} \leftarrow 12_{10}$	905 929	0.3
$13_{10} \leftarrow 13_{10}$	905 933	0.4
$14_{10} \leftarrow 14_{10}$	905 937	0.2
$11_{11} \leftarrow 11_{11}$	906 038	−0.4
$12_{11} \leftarrow 12_{11}$	906 042	0.4
$13_{11} \leftarrow 13_{11}$	906 046	0.5
$14_{11} \leftarrow 14_{11}$	906 051	0.5
$15_{11} \leftarrow 15_{11}$	906 054	−0.9
$12_{12} \leftarrow 12_{12}$	906 165	−0.3
$13_{12} \leftarrow 13_{12}$	906 170	0.2
$14_{12} \leftarrow 14_{12}$	906 174	0.5
$13_{13} \leftarrow 13_{13}$	906 303	−0.2
$14_{13} \leftarrow 14_{13}$	906 308	0.3
$15_{13} \leftarrow 15_{13}$	906 313	0.7
$16_{13} \leftarrow 16_{13}$	906 318	0.3
$17_{13} \leftarrow 17_{13}$	906 322	−0.5
$14_{14} \leftarrow 14_{14}$	906 452	−0.5
$15_{14} \leftarrow 15_{14}$	906 458	0.3
$16_{14} \leftarrow 16_{14}$	906 463	0.6
$15_{15} \leftarrow 15_{15}$	906 612	−0.6
$16_{15} \leftarrow 16_{15}$	906 618	0.1
$17_{15} \leftarrow 17_{15}$	906 623	0.4
$16_{16} \leftarrow 16_{16}$	906 784	−0.8
$17_{16} \leftarrow 17_{16}$	906 790	0.1
$18_{16} \leftarrow 18_{16}$	906 795	0.4
$1_0 \leftarrow 0_0$	908 870	−0.4
$2_1 \leftarrow 1_1$	912 378	−0.5
$3_2 \leftarrow 2_2$	915 897	0.0
$3_1 \leftarrow 2_1$	915 881	0.0
$3_0 \leftarrow 2_0$	915 876	0.0
$4_3 \leftarrow 3_3$	919 427	0.0
$4_2 \leftarrow 3_2$	919 400	0.2
$4_1 \leftarrow 3_1$	919 384	0.4
$5_4 \leftarrow 4$	922 968	0.4
$5_3 \leftarrow 4_3$	922 931	0.7
$5_2 \leftarrow 4_2$	922 903	0.5
$5_1 \leftarrow 4_1$	922 887	0.7
$5_0 \leftarrow 4_0$	922 882	0.7
$6_5 \leftarrow 5_5$	926 520	0.1
$6_4 \leftarrow 5_4$	926 473	2.3
$6_3 \leftarrow 5_3$	926 433	0.5
$6_2 \leftarrow 5_2$	926 402	−3.4

Table 1 (continued)

$J'_\kappa \leftarrow J''_\kappa$	Frequency (MHz)	Residual
$6_0 \leftarrow 5_0$	926 384	0.7
$7_6 \leftarrow 6_6$	930 083	−0.2
$7_5 \leftarrow 6_5$	930 023	0.0
$7_4 \leftarrow 6_4$	929 974	0.4
$7_3 \leftarrow 6_3$	929 935	0.1
$7_2 \leftarrow 6_2$	929 908	0.4
$7_1 \leftarrow 6_1$	929 892	0.1
$7_0 \leftarrow 6_0$	929 886	0.2
$8_7 \leftarrow 7_7$	933 656	−0.5
$8_6 \leftarrow 7_6$	933 585	−0.1
$8_5 \leftarrow 7_5$	933 525	0.0
$8_4 \leftarrow 7_4$	933 476	0.1
$8_3 \leftarrow 7_3$	933 437	−0.1
$8_2 \leftarrow 7_2$	933 410	0.1
$8_1 \leftarrow 7_1$	933 393	−0.2
$8_0 \leftarrow 7_0$	933 388	0.0

Residuals are observed frequencies minus those calculated from the parameters in Table 2.

was used to fit the data and determine the rotational parameters shown in Table 2. Here, ν is the vibrational origin, B and C are the unique symmetric rotor rotational constants, and D_J and D_{JK} are quartic centrifugal distortion parameters. The upper- and lower-state centrifugal distortion constants, D_J and D_{JK}, were constrained to be equal ($D''_J = D'_J$, $D''_{JK} = D''_{JK}$) in the fit due to large correlations when they were varied independently. Because a $\Delta K = 0$ symmetric rotor spectrum does not allow independent determination of the B_z-rotational constant (the C-constant of an oblate rotor), only the difference between upper- and lower-state C-constants could be determined from the data. The lower-state B-rotational constant is within 1 MHz (0.05%) of that determined for the 81.2 cm^{-1} band. Although a simultaneous fit of (1) to both the 30.2 cm^{-1} and 81.2 cm^{-1} bands was undertaken under the assumption that the two might share a common lower state, and indeed yielded results consistent with that assumption, it is important to note that there is only one piece of information, viz. the B-rotational constant, linking the two states. Without knowledge of the ground-state C-rotational constants (C'') of both bands, the present data cannot resolve with certainty whether the two bands arise from a common lower vibrational level. Indeed, lower vibrational states
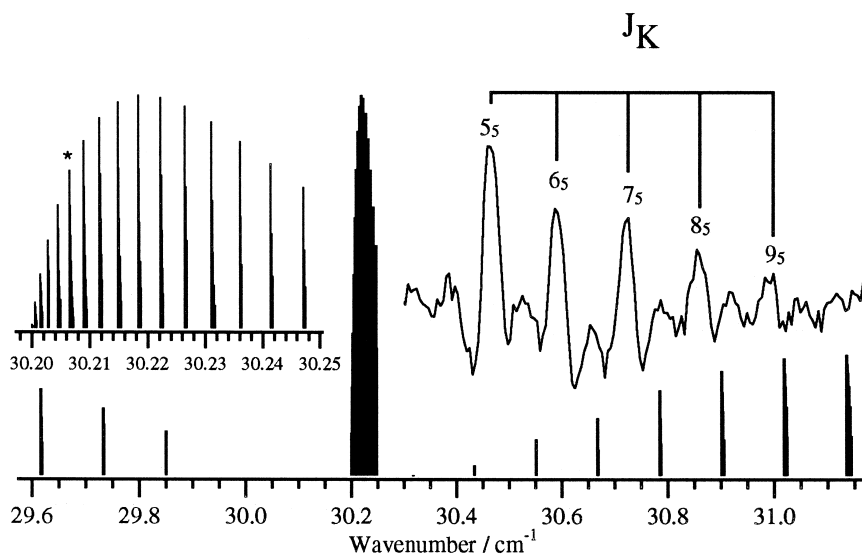
Fig. 2. The FIR–VRT spectrum of $(D_2O)_5$ observed near 30.2 cm^{-1}, shown as a stick spectrum. The intensities were calculated using a Boltzmann rotational distribution reflecting a rotational temperature of 5 K, with symmetric top Hönl–London factors. A blowup of the Q-branch region is shown on the left. The relative experimental intensities in this region are more reliable than for the P- and R-branches due to the compactness of the transitions. The $K = 5$ Q-sub-branch is shown on the right. The Q-branch consists of clusters of lines corresponding to a given K, with $J'' = J' = K$, $K + 1$, and so on. The experimental line widths in the 30.2 cm^{-1} spectrum are 800 kHz, compared to 1.5 MHz measured in the 81.2 cm^{-1} pentamer spectrum.

wherein the B-constants are very similar, but the C''-constants differ markedly, have been observed in VRT spectra of $(D_2O)_3$ [16]. For comparison with theoretical intensity calculations, we note finally that the 30.2 cm^{-1} spectrum is less than half as intense as that observed at 81.2 cm^{-1}, when scaling for sensitivity in the two regions is considered (different FIR detectors were used). Signal-to-noise ratios were

20:1 at best for the strongest Q- and R-branch transitions in the 30.2 cm^{-1} spectrum.

3. C-constant estimate

A complete picture of the vibrationally averaged ground-state pentamer structure, including a more reliable estimate of R_{OO}, depends on a determination of the C''-rotational constant. Because no perpendicular ($\Delta K = \pm 1$) spectrum, which would allow independent measurement of the ground- and upper-state C-constants, has yet been observed, an effort was undertaken to estimate C'' from careful relative intensity measurements. Liu and coworkers [2] have already shown that the Q-branch intensity profile of the 81.2 cm^{-1} spectrum is most consistent with a planar or at least very nearly planar ground-state structure.

The $K = 5$ Q-sub-branch of the 30.2 cm^{-1} spectrum is reproduced in Fig. 2. Several such clusters of lines corresponding to $K'' \rightarrow (K' = K'')$ transitions with $J = K$, $K + 1$, $K + 2$, and so on ($J \equiv J'' = J'$),

Table 2
Rotational parameters (MHz) of the 30.2 cm^{-1} band obtained from a fit of Eq. (1) to the data in Table 1

Parameter	30.2 cm^{-1} band	81.2 cm^{-1} band
B''	1750.964(20)	1750.815(76)
D_j''	0.00324(23)	0.00159(48)
D_{jk}''	−0.00691(62)	−0.0048(15)
ν	905 368.415(89)	2 434 074.36(55)
B'	1751.116(20)	1751.163(76)
D_j'	$(= D_j'')$	0.00163(48)
D_{jk}'	$(= D_{jk}'')$	−0.0048(15)
$C'' - C''$	2.42156(85)	7.6155(86)

The rotational parameters of the 81.2 cm^{-1} band observed by Liu et al. [2] are included for comparison

were observed in a 1.4 GHz (0.05 cm^{-1}) wide region centered near the band origin. Due to the compactness of those sub-branches, relative intensities are less likely to be contaminated by the power fluctuations inherent in the FIR laser spectrometer than are those of more widely spaced lines. Reasonably precise rotational temperatures can be obtained from such intensity profiles. The strategy undertaken, therefore, was to map out a rotational temperature profile, $T_{rot}(K)$ as a function of the K-quantum number using these condensed Q-branch clusters. These progressions consist of transitions with the same K'', therefore the relative intensities are independent of C''. Ideally, it would be preferable to determine a functional form of $T_{rot}(K)$ from the temperature profile. For such a determination, however, more reliable temperatures would be needed. The results of the rotational temperature analyses for several of the Q-branch sub-bands are shown in Fig. 3a. Although the temperatures showed some K dependence, the trend was not clear enough to determine a functional form of $T_{rot}(K)$, therefore the average rotational temperature, $\bar{T} = 5.25$ K was used. This temperature is consistent with previous measurements of similar intensity profiles obtained using the pulsed slit nozzle.

The strong $J = K$ Q-branch progression, characteristic of a planar oblate molecule, was least squares

fit to determine C'' from the relative intensity expression

$$I_{rel}^{\Delta J = \Delta K = 0} = \frac{(2J+1)K^2}{J(J+1)} 2(J+1)$$

$$\times \exp\left(-\frac{BJ(J+1) - (C'' - B)K^2}{k\bar{T}_{rot}}\right) \tag{2}$$

where B is the ground-state rotational constant given in Table 2, and C'' is determined as an adjustable parameter. The first term in (2) is the symmetric-top Hönl–London factor for $\Delta K = \Delta J = 0$ transitions [17], and k is the Boltzmann constant.

Fig. 3b shows the result of the fit of (2) to the $J = K$ Q-branch intensity profile. The C''-constant obtained in this analysis is 975 ± 60 MHz (1σ), consistent with the theoretical predictions of a quasi-planar oblate rotor, where $2C \approx B$. The value of C'' obtained in this manner is extremely (exponentially) sensitive to the choice of T_{rot} and can only bracket the vibrationally averaged structure to lie near that of the theoretical consensus. We estimate that including the standard deviation of the rotational temperature would be equivalent to adding an error of 8% to the relative intensity measurements.
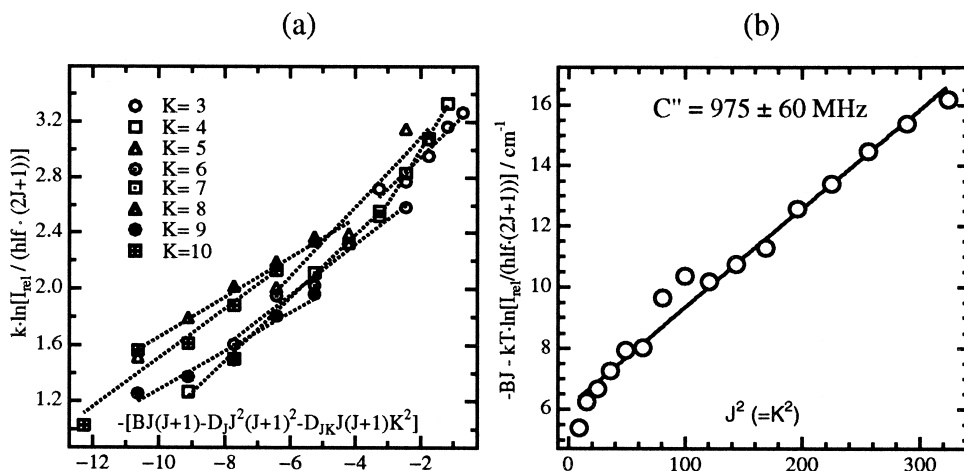

Fig. 3. (a) Plots of the relative intensities of several of the Q-sub-branches. The lines are the results of linear least squares fits to Hönl–London factor weighted Boltzmann distributions to yield T_K, the rotational temperatures as a function of the K-quantum number. (b) Fit of Eq. (2) to the strong $J = K$ Q-branch progression. An average rotational temperature of 5.25 K was assumed.

4. Absence of tunneling fine structure

It is known that the characteristic quartet splitting patterns observed in all seven of the measured $(D_2O)_3$ and $(H_2O)_3$ VRT spectra arise from 'bifurcation' or 'donor tunneling,' wherein the bound and free protons of one monomer exchange roles [3]. A simple extension of the group theoretical analysis that led to that conclusion predicts that each rotational transition of similar cyclic water clusters could be split into as many as $n + 1$ transitions, where n is the number of monomers in the cluster. This has not been observed, however, in either the VRT spectra of $(D_2O)_4$ or $(D_2O)_5$ where only doublet or singlet transitions are observed, respectively. Wales and Walsh [18] have performed tunneling pathway calculations for the pentamer, similar to those which have

provided much insight into the trimer dynamics, and have indeed found a feasible pathway which could lead to spectral splittings.

The lower-frequency pentamer spectrum provides a more rigorous test of whether any splittings are present. Although the Doppler limited line width at 30 cm^{-1} is 2.7 times narrower than that at 82 cm^{-1}, no substructure was observed in any of several carefully analyzed transitions. Alignment of the multipass cell used in the VRT experiments requires some degree of non-orthogonal intersection of the laser sidebands with the nozzle expansion, which is certain to cause additional Doppler broadening. Consequently, additional experiments were performed, passing the FIR radiation only once through and orthogonal to the planar expansion, thus minimizing the Doppler line width contribution imposed by the optical arrangement. Fig. 4 shows scans of a single Q-branch transition recorded over a range of frequency modulation (FM) deviations. We can conclude from the results that, to within the Doppler limited resolution of the experiment (≈ 450 kHz), there is no substructure in the observed transitions. Similar results were obtained when other transitions, including P- and R-branch lines, were examined in this manner.
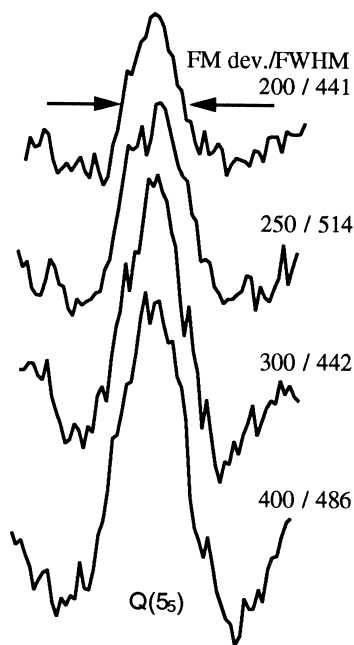
5. Discussion

Within the limits imposed by the interpretation of a $\Delta K = 0$ VRT spectrum, the vibrationally averaged water pentamer structure determined from this and the previous study [2] is consistent with theoretical predictions of a cyclic quasiplanar equilibrium structure. The pentamers observed in the VRT experiments correspond to a symmetric top with C_{5h} dynamical symmetry via averaging over the facile H-bond torsional motions and probably heavy atom (oxygen) motions as well. The approximate C''-rotational constant obtained from the intensity profiles in the Q-branch region is further evidence for a near planar equilibrium structure, where $2C \approx B$. Observation of a $\Delta K = \pm 1$ spectrum will provide a necessary and important clue about the vibrationally averaged structure, and further search efforts are currently underway.

Fig. 4. Doppler limited scans of the $5_5 \leftarrow 5_5$ transition (905 507 MHz) at a variety of frequency modulation deviations reveal no substructure to within the 450 kHz (FWHM) line width. Each scan consists of 60 data points which are each the average of 240 nozzle pulses using Ar carrier gas. The top trace is the average of 10 scans while the lower traces are each an average of five scans. Similar results were obtained when other transitions, including P- and R-branch lines, were examined.

Liu and coworkers [2] were unable to induce Stark splittings in a variety of transitions in the 81.2 cm^{-1} spectrum, consistent with other electric field deflection results [19], Although Wales [17] has calculated an equilibrium dipole moment of 0.847 D, this will be greatly reduced by the vibrational averaging effect of 'flipping' motions. Haberland and coworkers [20] were able to attach low-energy electrons to jet cooled $(H_2O)_n$ and $(D_2O)_n$ for n up to 90, except for $n = 4$. While large negative ion signals were obtained for $n = 2$ and $n = 6$, no signal was observed for the water tetramer and weak signals were observed for $(H_2O)_5^-$ and $(D_2O)_5^-$. The absence of a tetramer signal has been rationalized by observation [7] of a quasiplanar tetramer for which S_4 equilibrium point group symmetry, which would yield a zero equilibrium dipole moment, has been proposed. The pentamer observation is consistent with an equilibrium dipole moment near or above the theoretical (classical) threshold for electron attachment [21], approximately 1.6 D.

Bifurcation tunneling fine structure, anticipated in the pentamer VRT spectra by analogy with the water trimer, is absent in both of the $(D_2O)_5$ bands recorded thus far. Doppler limited experiments have revealed no additional splittings of the vibration–rotation transitions to within a precision of about 450 kHz. There are two possible explanations for the observation: (1) bifurcation tunneling is quenched in the pentamer to within the resolution of the VRT experiments, or (2) the differences between upper- and lower-state tunneling splittings are smaller than the experimental resolution. The first possibility is partially rationalized by the data and by theoretical predictions. The centrifugal distortion constants, D_J and D_{JK}, necessary to fit Eq. (1) to the data are an order of magnitude smaller than those needed to fit similar expressions to the water dimer and trimer data. Although caution must be observed in imparting physical significance to these parameters in the case of highly non-rigid molecules — they are often 'contaminated' by the dynamics, the results do imply a relatively more rigid pentamer framework. Theoretical predictions have shown that H-bonds in the pentamer are stronger than in smaller water clusters due to both increased contributions from many-body interactions and nearly optimal (tetrahedral) H-bonding angles.

Using the diffusion quantum Monte Carlo (DQMC) technique they implemented to study tunneling splittings in the water dimer and trimer, Gregory and Clary calculated the ground-state tunneling splittings due to H-bond torsional and bifurcation tunneling in the pentamer [22–27]. They adapted the anisotropic site potential (ASP) of Millot and Stone [28] to include an iterated many-body induction term [29] and a many-body dispersion interaction [30], and calculated bifurcation tunneling splittings of 70 and 220 MHz for $(D_2O)_5$ and $(H_2O)_5$, respectively. They noted that the calculated splittings are a factor of two smaller than splittings they calculated for $(D_2O)_3$ with an identical method [25]. Because the largest observed bifurcation tunneling splittings in $(D_2O)_3$ were no larger than 5 MHz, it seems reasonable that bifurcation might not be manifested in the $(D_2O)_5$ VRT spectra to within the resolution of the experiment. The H-bond torsional tunneling splitting calculated by those authors, 100 times smaller in $(D_2O)_5$ than in $(D_2O)_3$, is more difficult to rationalize. They argued that the combination of the length of the reaction path, and that in order for the motion to interconvert degenerate structures oxygen atom motion must occur, is sufficient rationale for the small splittings. It is difficult to gauge the effect of the latter argument, however, because there is actually no a-priori evidence that significant oxygen motion does *not* take place in the water trimer flipping dynamics. This is due to the fact that the three oxygens of the trimer form a plane by definition. Moreover, Viant and coworkers [31] have shown, using isotopic substitution experiments, that the flipping motion must be coupled with bound proton or deuteron motion. It seems more likely that the small flipping splittings calculated by Gregory and Clary are artifacts of the ASP potential surface or its many-body correction. Wales' recent calculations [18] have predicted zero-point energy corrected barriers to bifurcation tunneling and flipping in the pentamer of 577 and < 0 cm^{-1}, respectively. The corresponding barriers in water trimer [4] are 381 and < 0 cm^{-1}.

Some of Xantheas' ab initio (HF) results [9] are reproduced in Table 3, which shows that the fraction of total stabilization energy follows the degree of H-bonding linearity in the cyclic clusters. From a purely geometric point of view, the linearity of the

Table 3

Selected results (kcal mol^{-1}) from Xantheas' HF ab initio calculations [31] of the structures and energetics, including non-additive contributions, of cyclic water clusters ($n = 3$–5) and the dimer

	$n = 2$	$n = 3$	$n = 4$	$n = 5$
ΔE_{stab}	-3.71	-11.00	-19.51	-25.93
$\Delta E_{stab}/n$	-1.86	-3.67	-4.88	-5.19
%$\Delta E_{relaxation}$	-0.4	-1.1	-1.4	-1.4
%$\Delta E(2)$	100.4	88.6	82.2	78.9
%$\Delta E(3)$		12.5	18.1	20.4
%$\Delta E(4)$			1.1	2.1
%$\Delta E(5)$				0.01
$R_{OO}/\text{Å}$	3.03	2.93	2.88	2.87
$\delta(OH \cdots O)$	$175°$	$149°$	$174°$	$178°$

Although higher level (MP2, MP4) calculations were performed, only HF results were available for the pentamer. The trends in the higher level calculation are reasonably well preserved in the HF level results.

ΔE_{stab} is the total stabilization energy and $\Delta E_{stab}/n$ is the per monomer energy. $\Delta E(n)$ is the contribution (%) of n-body intermolecular forces to the stabilization energy and $\delta(OH \cdots O)$ is the H-bonding angle.

Mihn and coworkers [32] have calculated the per-monomer well depth (D_0) and binding energy (D_e) at one of the highest levels of ab initio theory (HF structural optimization with MP2/BSSEC, DZP basis). They predicted $D_0(D_e) = -3.38(-5.19)$ and $-5.26(-7.37)$ for the trimer and pentamer, respectively. (Those authors also calculated the trimer energies with MP2 structural optimization and obtained $D_0 = -3.11$ and $D_e = -5.10$ kcal mol^{-1}.)

H-bonding angle increases to a maximum for the cyclic pentamer, i.e. the bonds are less strained. There is general agreement in that the dominant source of many-body interactions in cyclic water clusters arises from mutually reinforced induction forces, which are at a maximum when the H-bond angles are linear. The trend is illustrated by the results in the table. For the pentamer, ~ 16% of the total stabilization energy arises from non-nearest neighbor two-body interactions, while three-body forces account for ~ 20% of the total, and higher-order interactions are dramatically less important. It seems clear that an understanding of such three-body interactions will be necessary to assemble a complete picture of the bulk phases of water.

As emerging data on the water trimer has shown, small water clusters are providing detailed knowledge about the microscopic interactions of water molecules in liquid and solid water. The water pentamer presents a system in which the effects of many-body intermolecular forces are quite possibly at a maximum due to the geometry of the cluster, and thereby provides an excellent opportunity to examine the nature of these interactions. Further spectroscopic studies are presently underway as an aid to better understand these effects in the pentamer.

References

[1] I. Ohmine, J. Phys. Chem. 99 (1995) 6767, and references therein.

[2] K. Liu, M.G. Brown, J.D. Cruzan, R.J. Saykally, Science 271 (1996) 62.

[3] K. Liu, J.G. Loeser, M.J. Elrod, B.C. Host, J.A. Rzepiela, R.J. Saykally, J. Am. Chem. Soc. 116 (1994) 3507.

[4] D.J. Wales, J. Am. Chem. Soc. 115 (1993) 11180.

[5] M. Schütz, T. Bürgi, S. Leutwyler, J. Chem. Phys. 99 (1993) 5228.

[6] A. Van der Avoird, E.H.T. Olthof, P.E.S. Wormer, J. Chem. Phys. 105 (1996) 8034.

[7] J.D. Cruzan, L.B. Braly, K. Liu, M.G. Brown, J.G. Loeser, R.J. Saykally, Science 271 (1996) 59.

[8] J.D. Cruzan, M.G. Brown, K. Liu, L.B. Braly, R.J. Saykally, J. Chem. Phys. 105 (1996) 6634.

[9] S.S. Xantheas, T.H. Dunning Jr., J. Chem. Phys. 99 (1993) 8774.

[10] B.J. Mhin, J. Kim, S. Lee, J.Y. Lee, K.S. Kim, J. Chem. Phys. 100 (1994) 4484.

[11] G. Chalasiski, M. Szczesniak, P. Cieplak, S. Scheiner, J. Chem. Phys. 94 (1991) 2873.

[12] K. Liu, J.D. Cruzan, R.J. Saykally, Science 271 (1996) 877.

[13] G.A. Blake, K.B. Laughlin, R.C. Cohen, K.L. Busarow, D.-H. Gwo, C.A. Schmuttenmaer, D.W. Steyert, R.J. Saykally, Rev. Sci. Instrum. 62 (1991) 1693.

[14] K. Liu, R.F. Fellers, M.R. Viant, R.P. McLaughlin, M.G. Brown, R.J. Saykally, Rev. Sci. Instrum. 67 (1996) 410.

[15] D.R. Herriott, H.J. Schulte, Appl. Opt. 4 (1965) 883.

[16] M.R. Viant, J.D. Cruzan, M.G. Brown, R.J. Saykally, in preparation.

[17] R.N. Zare. Angular Momentum: Understanding Spatial Aspects in Chemistry and Physics, Wiley Interscience, New York, 1988.

[18] D.J. Wales, T.R. Walsh, J. Chem. Phys. 105 (1996) 6957.

[19] T.R. Dyke, J.S. Muenter, J. Chem. Phys. 57 (1972) 5011.

[20] H. Haberland, C. Ludewigt, H.-G. Schindler, D.R. Worsnop, Surf. Sci. 156 (1985) 157.

[21] W. Garrett, J. Chem. Phys. 71 (1979) 651.

[22] J.K. Gregory, D.C. Clary, Chem. Phys. Lett. 228 (1994) 547.

[23] J.K. Gregory, D.J. Wales, D.C. Clary, J. Chem. Phys. 102 (1995) 1592.

[24] J.K. Gregory, D.C. Clary, J. Chem. Phys. 103 (1995) 8924.

[25] J.K. Gregory, D.C. Clary, J. Chem. Phys. 102 (1995) 7814.

[26] J.K. Gregory, D.C. Clary, Chem. Phys. Lett. 237 (1995) 39.

[27] J.K. Gregory, D.C. Clary, J. Phys. Chem. 100 (1996) 18014.

[28] C. Millot, A.J. Stone, Mol. Phys. 77 (1992) 439.

[29] A.J. Stone, Mol. Phys. 56 (1985) 1065.

[30] B.M. Axilrod, E. Teller, J. Chem. Phys. 11 (1943) 299.

[31] M.R. Viant, J.D. Cruzan, D.D. Lucas, K. Liu, M.G. Brown, R.J. Saykally, J. Phys. Chem. (1998) in press.

[32] B.J. Mhin, S.J. Lee, K.S. Kim, Phys. Rev. A 48 (1993) 3764.